

Cite this article as: Li Yuanyuan, Zhang Ziyi, Guan Jiahao, et al. Effect of Low-Dose Al Doping on Structure and Optical Properties of Sputtered SnO₂ Thin Films on Slide Glass[J]. Rare Metal Materials and Engineering, 2021, 50(05): 1513-1517.

ARTICLE

Effect of Low-Dose Al Doping on Structure and Optical Properties of Sputtered SnO₂ Thin Films on Slide Glass

Li Yuanyuan¹, Zhang Ziyi¹, Guan Jiahao¹, Li Li¹, Li Shuli¹, Cheng Zhen¹, Yang Rui¹, Zhang Yunzhe¹, Zhao Xiaoxia¹, Xu Kewei^{1,2}

¹ Shaanxi Key Laboratory of Surface Engineering and Remanufacturing, Xi'an University, Xi'an 710065, China; ² Nano-film and Biological Materials Research Center, Xi'an Jiaotong University, Xi'an 710049, China

Abstract: A series of SnO₂ thin films doped with low-dose Al (≤ 1 mol%) were prepared on slide glass substrates by radio frequency (RF) magnetron sputtering. The crystal structure and optical properties were investigated by X-ray diffraction (XRD), scanning electron microscopy (SEM), UV-IR spectrometer, and photoluminescence (PL) measurements. Results show that the lattice constant c decreases with increasing the Al content, which implies that Al atoms are successfully introduced into the SnO₂ and occupy the Sn sites, and large number of oxygen vacancies are generated. The average transmittance values are higher than 88% within the visible spectral region (400~800 nm) for all the films. The bandgap broadens when the Al percentage increases, which is dominated by the Burstein-Moss (BM) effect. The PL spectra of these films have near band edge and deep level emission under the radiation excitation of 265 nm wavelength. The observed intensity of these peaks increases consistently with increasing the Al percentage.

Key words: SnO₂ thin films; radio frequency (RF) magnetron sputtering; crystal structure; optical properties

Doped and undoped tin oxide (SnO₂) nanomaterials have attracted a lot of attention^[1-9] due to its applications in photovoltaic devices^[4,5], flat panel displays^[6], solid-state sensors^[7-10], thin-film transistors^[11], and high order harmonic generations^[12]. Cation valences and adjustable oxygen deficiency are the bases to create and tune the chemical and physical properties of SnO₂ for novel applications. Many dopants have been used to improve the properties of SnO₂ for practical using^[13], such as Mo^[14], Al^[15-17], Ta^[18], In^[19], F^[20-22] and Sb^[23-25]. Doped SnO₂ thin films with nanostructure show increasing popularity in electrical and optical device applications^[1-4,6-19,25,26]. Many techniques, including spray pyrolysis^[2,3,15-17], magnetron sputtering^[6,11,19,25], sol-gel^[8], rheotaxis growth^[14], thermal oxidation^[14], and chemical vapor deposition (CVD)^[7,18], have been used to fabricate these thin films. Among these methods, the magnetron sputtering deposition has the advantages of easy operation, controllable film thickness, high purity, high speed, low temperature, and favorable adhesion on the substrates^[6,11,19,25].

Many traditional oxide semiconductor thin films have the

disadvantages of high cost and durability due to inclusion of rare metal materials and weak chemical stability, respectively. Rare metal-free SnO₂-system, which has stable physical properties at high temperatures and under chemical environments, is a good choice to replace those traditional thin films. Tin oxide thin films usually have a wide bandgap ($E_g=3.6$ eV at 300 K), which indicates that they have excellent optical properties in the visible spectral range (400~800 nm). However, the undoped SnO₂ thin films commonly have a relatively high resistivity ($>10^{-1}$ $\Omega \cdot \text{cm}$)^[26-30]. To solve this problem, Al can be considered for the metallic dopant for SnO₂ thin films because Sn has the approximately same large orbit as In does, and Al with slightly small orbit creates a stable bond with oxygen^[26-30]. Research of preparation processes to fabricate SnO₂ materials continues its drive toward improving the performance of these semiconducting materials for electrical and optical devices. However, challenges still exist for improving the fabrication processes for various advanced applications. A further investigation is required to examine the effect of Al dopant on the op-

Received date: May 16, 2020

Foundation item: Xi'an Science and Technology Project (2019KJWL05)

Corresponding author: Li Yuanyuan, Ph. D., Professor, Shaanxi Key Laboratory for Surface Engineering and Remanufacturing, Xi'an University, Xi'an 710065, P. R. China, E-mail: liyynxcn@aliyun.com

Copyright © 2021, Northwest Institute for Nonferrous Metal Research. Published by Science Press. All rights reserved.

timization of SnO₂ films^[27,28].

Bagheri-Mohagheghi^[29] and Ahmed^[30] showed that the Al concentration can have a strong influence on the electrical and optical properties of SnO₂ thin films. The conduction type transition from n-type to p-type occurs when the critical Al dopant percentage is near 8%^[29] and 12.05%^[30], depending on the initial number of n-type carriers in the films. When Al content is lower than the critical percentage, SnO₂-Al films behave as an n-type material; when Al content is higher than the percentage, the films behave as a p-type material^[29,30]. The variation of structures, resistivity, and optical bandgap of the films with different Al percentages was also reported^[29,30]. However, the low-dose Al-doped SnO₂ films with distinct structure and optical properties were not discussed thoroughly in those reports.

In this research, with increasing the addition of low-dose Al³⁺ dopant in SnO₂ thin films, the lattice constant *c* decreases, and the bandgap broadens. These variations of the structure and optical properties are probably due to the generation of a large number of oxygen vacancies.

1 Experiment

SnO₂-Al thin film samples were prepared by radio frequency (RF) magnetron sputtering on 1 cm×1 cm slide glasses with a thickness of 1 mm. Four ceramic targets of SnO₂ separately doped with 0.05mol%, 0.25mol%, 0.5mol%, and 1mol% Al were used in experiments. The slide glass substrates were firstly cleaned in acetone, rinsed in deionized water, and dried with N₂ gas before loading into the chamber. The distance between the target and the substrate was ~50 mm. The base pressure was 4.0×10⁻⁴ Pa, and the film growth was carried out in the growth ambient with the ratio of oxygen to argon gas flow (mL/min) of 50:100. The target was pre-sputtered in pure Ar for 10 min to remove surface contamination and maintain system stability. The sputtering power at 80 W was maintained, and the target area was ~80 cm². So the power density applied on all the films was ~1 W/cm² for 2 h during sputtering. The four samples doped with 0.05mol%, 0.25mol%, 0.5mol%, and 1mol% Al were marked as SA-0.05, SA-0.25, SA-0.5, and SA-1, respectively, and were deposited on the substrates at 300 °C.

The XRD patterns were obtained by an X-ray diffractometer (Bruker D2 Phaser) using Cu Kα radiation (0.154 nm) at 40 kV and 40 mA. The micrographs of scanning electron microscope (SEM, JEOL JSM-6930A) were studied. The absorption/transmission and photoluminescence (PL) spectra were investigated by UV-vis-NIR spectrometer (HR4000) and Horiba FluoroMax-4, respectively.

2 Structure and Morphological Properties of SnO₂-Al Films

Fig. 1 shows the XRD patterns of all the films. The broad hump between 20° and 40° is the background intensity due to the glass substrates. The observed peak positions are corresponding to the rutile structure of polycrystalline SnO₂ films (JCPDS 41-1445). The lattice constants of four samples are shown in Table 1, which agree well with the reported bulk values *a*=0.4738 and *c*=0.3187 nm from the reference pattern.

As shown in Fig.1, (110) and (101) are the preferred orienta-

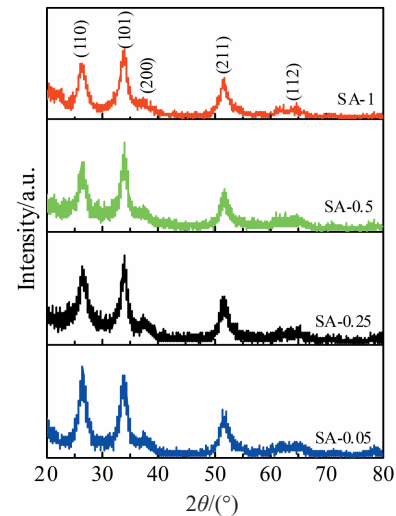


Fig.1 XRD patterns of SnO₂ thin films doped with different Al contents

Table 1 Crystalline parameters of the SA-0.05, SA-0.25, SA-0.5, and SA-1 films

Film	2θ/(°)	(hkl)	Lattice constant/nm	<i>d</i> _{hkl} /nm	<i>I</i> /%	<i>I</i> ₀ /%	<i>B</i> /(°)	<i>D</i> /nm
SA-0.05	26.281	(110)	-	0.3388	100.0	100	0.663	12.5
	33.600	(101)	<i>a</i> =0.4792	0.2665	93.2	75	0.831	10.1
	51.421	(211)	<i>c</i> =0.3190	0.1776	42.5	57	0.937	9.5
SA-0.25	26.318	(110)	-	0.3384	69.0	100	0.661	12.5
	33.723	(101)	<i>a</i> =0.4785	0.2656	100.0	75	0.600	14.0
	51.575	(211)	<i>c</i> =0.3173	0.1771	47.9	57	0.572	15.7
SA-0.5	26.359	(110)	-	0.3378	69.6	100	0.642	12.9
	33.996	(101)	<i>a</i> =0.4778	0.2635	100.0	75	0.682	12.3
	51.782	(211)	<i>c</i> =0.3143	0.1764	69.6	57	0.459	19.7
SA-1	26.320	(110)	-	0.3383	75.9	100	0.743	11.1
	34.080	(101)	<i>a</i> =0.4785	0.2629	100.0	75	0.885	9.2
	51.783	(211)	<i>c</i> =0.3131	0.1764	72.4	57	0.525	17.1

tions for all the films. Other orientations, such as (211), (200), and (112), also appear with relatively lower intensities. With lower doping level, the SA-0.05 film grows slightly faster along preferable plane (110) than that along (101). As the content of Al dopant increases, there is a gradual suppression of the growth along (110) plane. Instead, the films growth along (101) becomes faster than that along (110). Also, the decrease of lattice constant c from 0.3190 nm to 0.3131 nm indicates that more Al atoms with slightly small orbit are successfully introduced into the SnO₂ host and occupy the Sn sites, and the preferable peak of (110) shifts to the larger diffraction angles, i.e., (101) plane. This suggests that the lowest surface energy density along the (110) orientation in SnO₂ crystal transfers into (101) orientation with increasing the Al concentration^[13].

The grain sizes of samples are calculated (Table 1) by the Scherrer's equation^[31] as follows:

$$D=0.9\lambda/\beta\cos\theta \quad (1)$$

where λ is the X-ray wavelength of 0.154 nm, θ is the Bragg diffraction angle, and β is the full width at half maximum (FWHM) of the diffraction peaks. Besides, β is corrected by the Warren formula $\beta^2=B^2-b^2$, where B is the measured peak width and $b=0.1^\circ$ is the peak broadening due to the machine. The average calculated grain sizes of SA-0.05, SA-0.25, SA-0.5, and SA-1 films using the data of (110), (101), and (211) peaks, are 10.7, 14.1, 15.0, and 12.5 nm, respectively, which indicates that the crystalline quality of SnO₂ thin films improves with increasing the Al doping percentage.

The thickness of the films determined by the cross-section scan is ~430 nm (Fig.2). Considering that there is no apparent difference between all the films, the observed surface of the film is smooth and uniform with lower roughness due to the grain growing induced by large particle coalescence, which also confirms the good quality of thin film.

3 Optical Properties of SnO₂-Al Films

The UV-IR spectra of all samples are shown in Fig.3. The observed average transmittance values of all the films are higher than 88% within the visible region (400~800 nm), due to the improvement of the crystalline structures and surface quality^[32,33]. The sharp band edge absorption of thin films observed in Fig.3a is due to the quantum interaction of incident light and thin films. A shift of optical band edge towards the

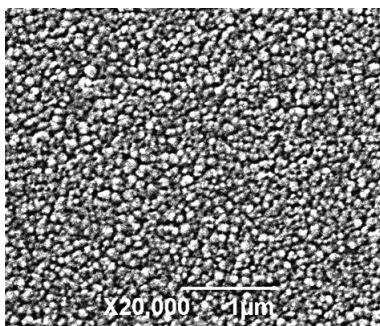


Fig.2 SEM image of SA-0.05 film

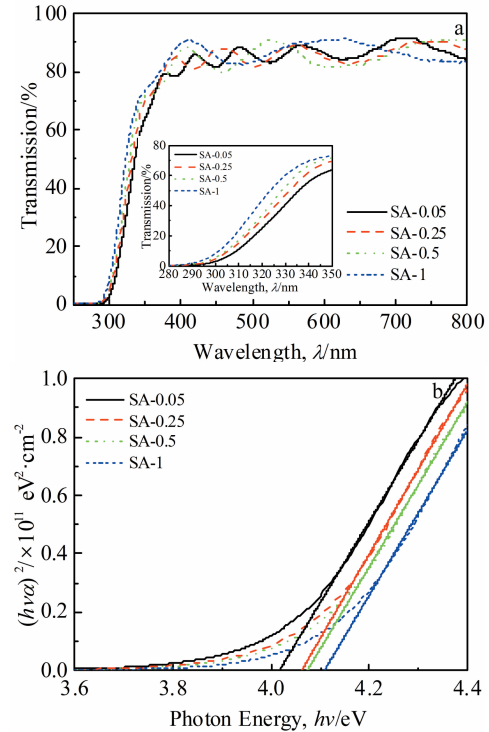


Fig.3 Transmission- λ (a) and $(h\nu)^2-h\nu$ (b) plots of SnO₂ thin films doped with different Al concentrations

short wavelength is also noticeable with increasing the Al dopant percentage. The absorption edge of the films, corresponding to electron transitions from the valence band to the conduction band, can be used to determine the optical band gap E_g of the films. The absorption coefficient can be expressed by Eq.(2)^[34]:

$$\alpha(h\nu) = C\sqrt{h\nu - E_g} \quad (2)$$

where C is a constant for a direct transition, α is the optical absorption coefficient, and $h\nu$ is the photon energy. The plots of $(h\nu)^2-h\nu$ are shown in Fig.3b. The gap values of SA-0.05, SA-0.25, SA-0.5, and SA-1 films obtained by extrapolating the linear absorption edge parts of the plots are about 4.02, 4.06, 4.07 and 4.11 eV, respectively. The bandgap broadens obviously with increasing the Al percentage. This bandgap broadening is dominated by the well-known Burstein-Moss (BM) shift^[35,36], as follows:

$$\Delta E = \frac{\hbar^2}{2m_{vc}^*} (3\pi^2 n)^{2/3} \quad (3)$$

where \hbar is the Plank constant, n is the present carrier concentration, m_{vc}^* is the reduced effective mass^[35,36], as follows:

$$m_{vc}^* = m_{vc}^* m_c^* / (m_v^* + m_c^*) \quad (4)$$

where m_v^* and m_c^* are the effective mass of carriers in valance and conduction bands, respectively.

To examine the bandgap broadening, the film type and carrier concentration are determined by Hall experimental measurements conducted under a magnetic field of 0.2 T. The result shows that the SA-0.05, SA-0.25, SA-0.5, and SA-1 films doped with low-dose Al are n-type films with the carrier concentration of $\sim 1.3 \times 10^{17}$, 4.9×10^{18} , 6.8×10^{18} , and 1.7×10^{19} cm⁻³,

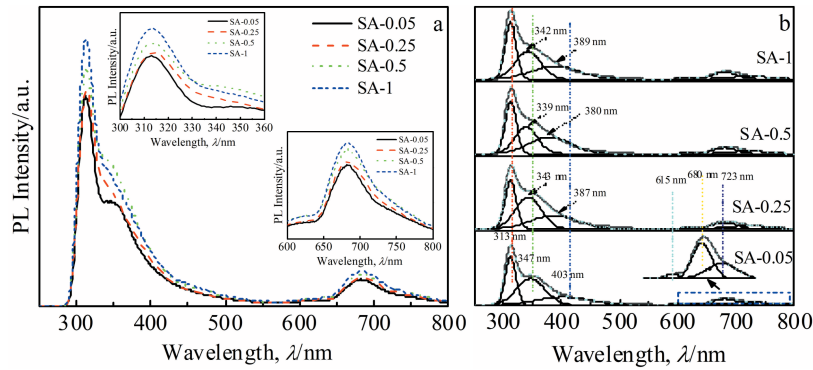


Fig.4 PL spectra (a) and Gaussian fitting lines (b) of SA-0.05, SA-0.25, SA-0.5, and SA-1 films

respectively. Although Al^{3+} is the acceptor doping in SnO_2 thin films due to the small radius of Al^{3+} (~ 0.051 nm)^[37], which is smaller than that of Sn^{4+} (~ 0.069 nm)^[38], the holes appear with broken bond induced by the substitution of Al in Sn sites. Large number of doubly ionized oxygen vacancies are generated^[39], so the majority carriers are still electrons whose concentration increases with increasing the low-dose Al dopants.

For tin-oxide based films, the bandgap shrinkage value induced by electron-electron and electron-impurity interactions is less than that of BM broadening^[40], so it is neglected in this discussion. Taking $m_v^* = m_0$ and $m_c^* = 3m_0$ ^[41], the shift value of the bandgap induced by BM effect is estimated as ~ 0.004 , 0.045 , 0.056 , and 0.10 eV for SA-0.05, SA-0.25, SA-0.5, and SA-1 films, respectively, which agrees with the experimental results.

Fig.4 shows the measured PL spectra and Gaussian fitting lines for all the films. The PL emissions were measured by a spectrometer Horiba FluoroMax-4 with an excitation wavelength of 265 nm at 150 W xenon pulse lamp. Several PL bands are used in the previous reports, including 564, 488, 417, 400, 387, and 370 nm^[42-45], and high-resolution peaks around 368–384 nm^[43]. These emission peaks are usually featured by a near band edge emission and a defect level emission in UV and visible regions, respectively. The Gaussian fit shows six symmetrical peaks centered at 313, ~ 347 , ~ 403 , 615, 680, and 723 nm accordingly. The first and the second emission peaks in the UV region is very close to the bandgap values of 4.02–4.11 eV, which indicates that these emissions are from the band and the near band edge. The observed peak in the UV band is much larger than that in the visible region, which implies a good crystallization quality of Al-doped SnO_2 thin films. With increasing the Al dopant concentration, more Al atoms occupy Sn atom sites in the lattice, and the carriers excited by UV light escape more easily from Al ions than those from Sn ions do. Therefore, a larger UV peak emerges due to the increase of excitonic recombination induced by a quick diffusion of excitons and more electron-hole pairs^[44]. The third emission peak is centered at 403, 387, 380, and 389 nm for SA-0.05, SA-0.25, SA-0.5, and SA-1 films, respectively. These peaks are ascribed to Sn interstitials in the films^[44]. The detailed peaks at 615, 680, and 723 nm are not yet very

clear. It is believed that these peaks are caused by the defect level emission induced by oxygen vacancies, which forms a considerable number of trapped states within the bandgap^[44]. Also, the decrease of lattice parameter c of the film suggests an increase in oxygen vacancies^[39], leading to the recombination of deeply trapped charges and photogenerated electrons from the conduction band, and the intensity of the peak thus increases with increasing the concentration of oxygen vacancies^[45]. It is apparent that the structure and optical properties of SnO_2 -Al thin films are not monotonous below or above the critical Al-doping concentration ($\sim 8.0\%$ ^[29] and $\sim 12.05\%$ ^[30]).

4 Conclusions

1) The lattice constant c decreases with increasing the Al content in SnO_2 films. It implies that Al atoms are successfully introduced into the SnO_2 host and occupy Sn sites, and a large number of oxygen vacancies are generated.

2) The UV-IR studies show that the average transmittance values are higher than 88% within the visible region (400–800 nm) for all the SnO_2 films with different Al contents. The bandgap broadens when the Al percentage increases, which is dominated by the Burstein-Moss (BM) effect.

3) The photoluminescence spectra of the SnO_2 films with different Al contents have near band edge and deep level emission under the radiation excitation of 265 nm wavelength. The intensity of the peaks increases with the increases of Al percentage. It is apparent that the structure and optical properties of SnO_2 -Al thin films are not monotonous below or above the critical Al-doping concentration ($\sim 8.0\%$ ^[29] and $\sim 12.05\%$ ^[30]). A further investigation is required to examine the effect of Al-doping percentage on the optimization of SnO_2 films.

References

- 1 Granqvist C G, Hultaker A. *Thin Solid Films*[J], 2002, 411(1): 1
- 2 Bagheri-Mohagheghi M, Shokooh-Saremi M. *Thin Solid Films*[J], 2003, 441(1-2): 238
- 3 Bagheri-Mohagheghi M, Shokooh-Saremi M. *Physica B: Condensed Matter*[J], 2010, 405(19): 4205
- 4 Lozano A E, Abajo J, De la Campa J G et al. *J Appl Polym Sci*[J],

- 2007, 103(6): 3491
- 5 Fung M K, Sun Y C, Ng A et al. *ACS Appl Mater Inter*[J], 2011, 3(2): 522
- 6 Betz U, Olsson M, Marthy J et al. *Surf Coat Technol*[J], 2006, 200(20-21): 5751
- 7 Singhal A V, Chandra K, Agarwala V. *Int J Nanotechnol*[J], 2015, 12(3-4): 248
- 8 Kumar M, Kumar A, Abhyankar A. *ACS Appl Mater Inter*[J], 2015, 7(6): 3571
- 9 Liu G, Wang Z, Chen Z et al. *Sensors*[J], 2018, 18(4): 949
- 10 Peng M Y, Lv D W, Xiong D et al. *J Electron Mater*[J], 2019, 48(4): 2373
- 11 Zhang X, Lee H, Kim J et al. *Materials*[J], 2018, 11(1): 46
- 12 Capretti A, Wang Y, Engheta N et al. *Opt Lett*[J], 2015, 40(7): 1500
- 13 Batzill M, Diebold U. *Prog Sur Sci*[J], 2005, 79(2-4): 47
- 14 Zampiceni E, Bontempi E, Sberveglieri G et al. *Thin Solid Films* [J], 2002, 418(1): 16
- 15 Korotcenkov G, Borinzari V, Golovanov V et al. *Sens Actuators B Chem*[J], 2004, 98(1): 21
- 16 Mageto J, Mwamburi M, Muramba V. *Elixir Chem Phys*[J], 2012, 53: 11 922
- 17 Muramba V, Mageto M, Gaitho F et al. *Am J Mater Sci*[J], 2015, 5(2): 23
- 18 Lee S, Kim Y M, Chen H. *Appl Phys Lett*[J], 2001, 78(3): 350
- 19 Denny Y, Seo S, Lee K et al. *Mater Res Bull*[J], 2015, 62: 222
- 20 Esteves M, Gouvea D, Sumodjo P. *Appl Surf Sci*[J], 2004, 229(1-4): 24
- 21 Datta M, Kadakia K, Velikokhatnyi O I et al. *J Mater Chem A*[J], 2013, 1(12): 4026
- 22 Yang Y, Zhu B, Xie T et al. *J Chin Ceram Soc*[J], 2017, 45(4): 472 (in Chinese)
- 23 Egdell R, Walker T, Beamson G. *J Electr Spectr Rel Phenom*[J], 2003, 128(1): 59
- 24 Jain G, Kumar R. *Opt Mater*[J], 2004, 26(1): 27
- 25 Yang W H, Yu S H, Zhang Y et al. *Thin Solid Films*[J], 2013, 542: 285
- 26 Lin Y Y, Lee H Y, Ku C S et al. *Appl Phys Lett*[J], 2013, 102(11): 111 912
- 27 Chen Z, Pan D, Li Z et al. *Chem Rev*[J], 2014, 114(15): 7442
- 28 Belhamri S, Hamdadou N E. *Surf Rev Lett*[J], 2018, 25(4): 1 850 092
- 29 Bagheri-Mohagheghi M M, Shokooh-Saremi M. *J Phys D: Appl Phys*[J], 2004, 37(8): 1248
- 30 Ahmed S F, Khan S, P K Ghosh et al. *J Sol-Gel Sci Techn*[J], 2006, 39(6): 241
- 31 Yang X C. *Mater Sci Eng B*[J], 2002, 95(3): 299
- 32 Czaplak A, Kusior E, Bucko M. *Thin Solid Films*[J], 1989, 182(1-2): 15
- 33 Rakhshani A E, Makdisi Y, Ramazanyan H A. *J Appl Phys*[J], 1998, 83(2): 1049
- 34 Papadopoulou E L, Varda M, Kouroupis-Agalou K et al. *Thin Solid Films*[J], 2008, 516(22): 8141
- 35 Burstein E. *Phys Rev*[J], 1954, 93(3): 632
- 36 Moss T. *Proc Phys Soc London Sect B*[J], 1954, 67: 775
- 37 Weast C. *Hand Book of Chemistry, Physics*[M]. Boca Raton: CRC Press, 1985
- 38 Shannon R. *Acta Crystallographica Section A: Crystal Physics, Diffraction, Theoretical and General Crystallography*[J], 1976, 32(5): 751
- 39 Laurent P, Philibert I, Christophe P. *J Euro Ceram Soc*[J], 1999, 19(6-7): 747
- 40 Berggren K F, Sernelius B E. *Phys Rev B*[J], 1981, 24(4): 1971
- 41 Sanon G, Rup R, Mansingh A. *Phys Rev B*[J], 1991, 44(11): 5672
- 42 Hayakawa T, Enomoto T, Nogami M. *J Mater Res*[J], 2002, 17(6): 1305
- 43 Liu B, Cheng C W, Chen R et al. *J Phys Chem C*[J], 2010, 114(8): 3407
- 44 Nehru L C, Swaminathan V, Sanjeeviraja C. *Am J Mater Sci*[J], 2012, 2(2): 6
- 45 Jeong J, Choi S, Chang C I et al. *Solid State Commun*[J], 2003, 127(9-10): 595

微量 Al 掺杂对溅射于玻璃衬底的 SnO₂ 薄膜结构及光学特性的影响

李院院¹, 张子怡¹, 管佳豪¹, 李 莉¹, 李姝丽¹, 成 楨¹, 杨 睿¹, 张云哲¹, 赵小侠¹, 徐可为^{1,2}

(1. 西安文理学院 陕西省表面工程与再制造重点实验室, 陕西 西安 710065)

(2. 西安交通大学 纳米薄膜与生物材料研究中心, 陕西 西安 710049)

摘要: 采用射频 (RF) 磁控溅射法在玻璃衬底上制备了低浓度 Al 掺杂 ($\leq 1\text{mol}\%$) 的 SnO₂ 系列薄膜。通过 X 射线衍射、扫描电镜、紫外-红外光谱仪及光致发光 (PL) 实验, 展现了薄膜的晶体结构及光学特性。结果表明: 当 Al 浓度增加时, 薄膜晶格常数 c 减小, 表明 Al 原子成功替代 Sn 原子并产生了大量的氧空位。在 400~800 nm 的可见光范围, 薄膜的平均透射率可达 88% 以上。当 Al 浓度持续增加时, 由于 Burstein-Moss (BM) 效应使薄膜带隙增宽。此外, 测量发现, 在 265 nm 波长的光激发下, 所制备薄膜的 PL 谱具有典型的近边带和深能级辐射发光, 其峰值随 Al 浓度的增加而增大。

关键词: SnO₂ 薄膜; 射频磁控溅射; 晶体结构; 光学特性

作者简介: 李院院, 男, 1969 年生, 博士, 教授, 西安文理学院陕西省表面工程与再制造重点实验室, 陕西 西安 710065, E-mail: liy-yunxcn@aliyun.com.com